Impact of electrode roughness on metal-insulator-metal tunnel diodes with atomic layer deposited Al_2O_3 tunnel barriers

Nasir Alimardani, E. William Cowell III, John F. Wager, and John F. Conley, Jr.[a)]
School of EECS, Oregon State University, 1148 Kelley Engineering Center, Corvallis, Oregon 97331

David R. Evans
Sharp Laboratories of America, Inc., Camas, Washington 98607

Matthew Chin, Stephen J. Kilpatrick, and Madan Dubey
U.S. Army Research Laboratory, Adelphi, Maryland 20783

(Received 16 August 2011; accepted 12 October 2011; published 3 November 2011)

Metal-insulator-metal (MIM) tunnel diodes on a variety of high and low work function metals with various levels of root-mean-square roughness are fabricated using high quality atomic layer deposited Al_2O_3 as the insulating tunnel barrier. It is found that electrode surface roughness can dominate the current versus voltage characteristics of MIM diodes, even overwhelming the impact of metal work function. Devices with smoother bottom electrodes are found to produce current versus voltage behavior with higher asymmetry and better agreement with Fowler-Nordheim tunneling theory, as well as a greater percentage of functioning devices. © *2012 American Vacuum Society*. [DOI: 10.1116/1.3658380]

I. INTRODUCTION

Metal-insulator-metal (MIM)-based tunneling devices with very thin insulator layers compared to those of MIM capacitors have been proposed for a variety of applications, including hot electron transistors,[1,2] infrared (IR) detectors,[3,4] liquid-crystal display backplanes,[5] optical rectennas for IR energy harvesting,[6] and macroelectronics.[7] Despite investigation by many groups over many decades, progress toward the commercialization of MIM-based electronics has been hindered by the lack of a manufacturable process for the fabrication of high-quality MIM diodes. The operation of a MIM diode is based on quantum mechanical tunneling through a thin insulating film positioned between two metal electrodes.[8,9] The tunneling probability depends exponentially on the thickness of the insulator/insulator electric field; thus, the performance of a MIM tunnel diode should depend strongly on the atomic scale roughness and the uniformity of the electrode-insulator interfaces.[9–11] In fact, Miller *et al.*[12] have theoretically predicted that the interfacial roughness should affect the tunneling current in tunnel junctions. Inattention to the electrode roughness, along with the lack of a high-quality deposited oxide, appears to have slowed the development of this technology. Most experimental work to date on MIM diodes has focused on the use of thin native dielectrics produced by oxidation or nitridation of the underlying polycrystalline metal electrode.[1–4,13–17]

Basic studies on electrode and interface roughness and their correlation with the tunneling current will be very important for the advancement of MIM technology. Recently, we demonstrated that sputter deposition of the amorphous metal ZrCuAlNi can be used to produce an ultrasmooth electrode (~0.3 nm root-mean-square (RMS) roughness).[18] Although the use of ZrCuAlNi as a bottom electrode in conjunction with high-quality Al_2O_3 deposited via ALD allowed for the reproducible fabrication of MIM tunnel diodes, we were unable to make any functioning devices on very rough Al bottom electrodes. Although it was hypothesized that the reason for the good electrical characteristics on ZrCuAlNi, as opposed to the complete lack of functioning devices on Al, was due to the large difference in roughness, our previous work did not discuss the case of intermediate electrode roughness, in which the electrode roughness is not great enough to destroy all devices but is still large enough so that it might impact the electrical characteristics of functioning devices.

In the work presented herein, we compare MIM tunnel diode performance on low work function (ZrCuAlNi and Al) and high work function (Ir and two types of Pt) bottom electrode materials with various levels of RMS roughness. Whereas previous MIM diode work has focused primarily on native oxides, the use of atomic layer deposition (ALD) allows for the deposition of the same high-quality Al_2O_3 insulator on each of these bottom metal electrodes. We show that roughness can overwhelm the impact of the metal work function on the electrical characteristics of MIM diodes, in fact reversing the expected trends based on metal work functions. We also find that that the percentage yield of functioning devices tracks higher with decreasing roughness. Finally, we find that even for nominally the same metal (Pt), the level of roughness dominates the electrical characteristics and yield.

II. EXPERIMENT

MIM diodes were fabricated on Si substrates capped with 100 nm of thermally grown SiO_2. First, blanket films of Al, Pt, Ir, or ZrCuAlNi were deposited as bottom electrodes. A thin Ti adhesion layer was used for Pt and Ir. Al was deposited via thermal evaporation, Ir was deposited via electron-beam evaporation, and Pt was deposited using either dc sputtering (Pt-1) or electron-beam evaporation (Pt-2).

[a)]Electronic mail: jconley@eecs.oregonstate.edu

ZrCuAlNi was deposited via dc magnetron sputtering with no intentional substrate heating using a 3 in. diameter, 0.25 in. thick vacuum arc-melted metal target (with an atomic composition of $Zr_{40}Cu_{35}Al_{15}Ni_{10}$).[18] Next, a thin ($\lesssim 10$ nm) Al_2O_3 tunneling barrier was deposited via ALD using a Picosun SUNALE R-150B ALD reactor by alternating pulses of trimethlyaluminum (TMA) and de-ionized water at a temperature of 300 °C. Finally, top electrodes were formed by evaporating Al dots ($\sim$0.8 mm^2) through a shadow mask.

Current density-electric field (J-ξ) characterization was conducted using an Agilent 4156 C semiconductor parameter analyzer with samples at room temperature in the dark. The bottom electrode roughness (RMS and peak) was measured via atomic force microscopy (AFM) using a Digital Instruments 3 AFM with silicon-nitride tips. The work functions of bottom electrodes were measured in air over an area of approximately (1×1) mm^2 using a KP Technology SKP5050 scanning Kelvin probe with a 2 mm tip and calibrated against a gold standard. The work functions of ZrCuAlNi and Al were measured as approximately 4.8 eV and 4 eV, respectively. The thickness of Al_2O_3 films on ZrCuAlNi bottom electrodes was measured as 9.5 ± 0.5 nm via TEM assessment[18] and confirmed with a spectroscopic ellipsometer (J.A. Woollam Co. WVASE32) using a Cauchy model.

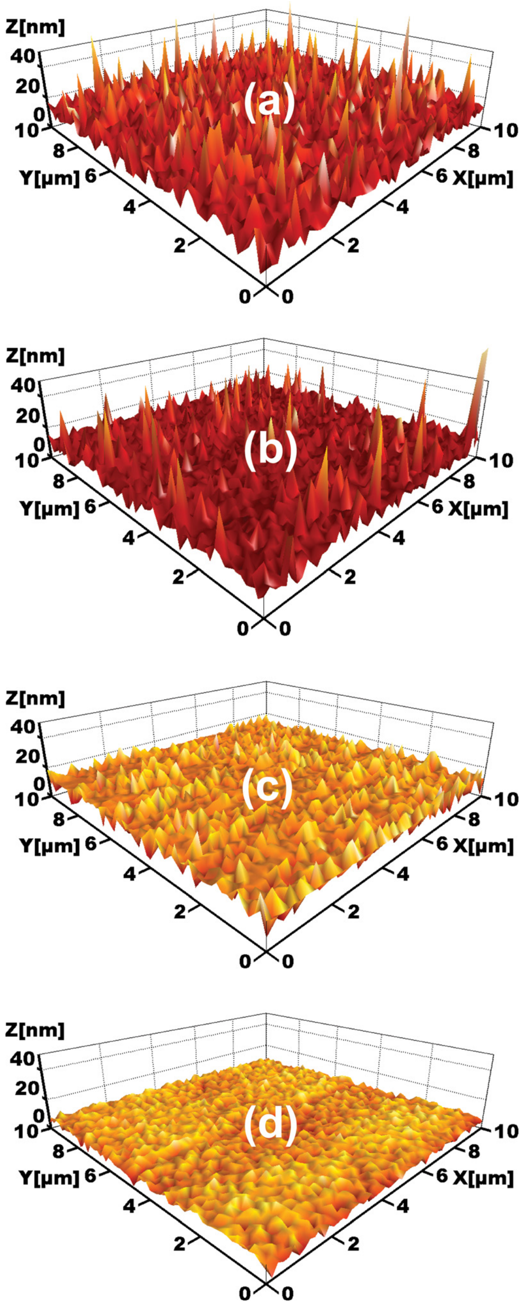

FIG. 1. (Color online) AFM micrographs of as-deposited (a) Ir, (b) electron-beam-deposited Pt-2, (c) sputtered Pt-1, and (d) ZrCuAlNi blanket bottom electrodes.

III. RESULTS AND DISCUSSION

AFM micrographs, shown in Fig. 1, were used to establish the RMS and peak roughness of as-deposited ZrCuAlNi, Pt-1, Pt-2, and Ir bottom electrodes. The roughness values are averaged from a minimum of three images each. In order to assess any potential roughening as a result of the ALD thermal cycle or interaction of the TMA precursor with the electrodes, additional AFM images were also taken after the deposition of a 10 nm Al_2O_3 layer (post-ALD). As summarized in Table I, the AFM images reveal wide variation in both RMS average roughness and peak roughness, with ZrCuAlNi having the lowest roughness by a factor of 10. With the exception of Pt-2, the RMS and peak roughness tend to scale together. Following Al_2O_3 deposition, roughness values did not significantly change for the smoothest as-deposited electrodes, whereas the RMS roughness improved for the roughest as-deposited electrode, Ir. In contrast, the Al electrodes were found to roughen by about a factor of 5 after the Al_2O_3 deposition. This increase in roughness is not due to the ALD Al_2O_3 deposition itself; rather, it is a consequence of the low melting point of Al and associated grain growth during the ALD thermal cycle.

Shown in Figs. 2(a) and 2(b) are simulated and representative measured J-ξ curves, respectively, for MIM devices with an Al top electrode (M_2); a $\sim$10 nm thick Al_2O_3 tunnel barrier; and Ir, Pt, or ZrCuAlNi as bottom electrodes (M_1). The J-ξ curves are simulated using the Fowler-Nordheim (FN) tunneling equations of Simmons,[9,11]

TABLE I. Work-function, roughness of various metal films, and percentage of functioning devices of metal bottom electrode/10 nm Al_2O_3/Al top electrode MIM tunnel diodes.

	Al	Pt-2	Ir	Pt-1	ZrCuAlNi
Work function (eV)	4	5.3	5.1	5.3	4.8
As-deposited RMS roughness (nm)	4	6 ± 1	11 ± 1	2 ± 0.5	0.3 ± 0.1
As-deposited Peak roughness (nm)	43	220 ± 5	120 ± 10	22 ± 5	3 ± 1
Post-ALD RMS roughness (nm)	21	5 ± 1	5 ± 1	2 ± 0.5	0.3 ± 0.1
Post-ALD Peak roughness (nm)	468	210 ± 10	130 ± 10	22 ± 10	3 ± 1
Functioning devices (%)	0	<10	30 to 40	30 to 50	65 to 80

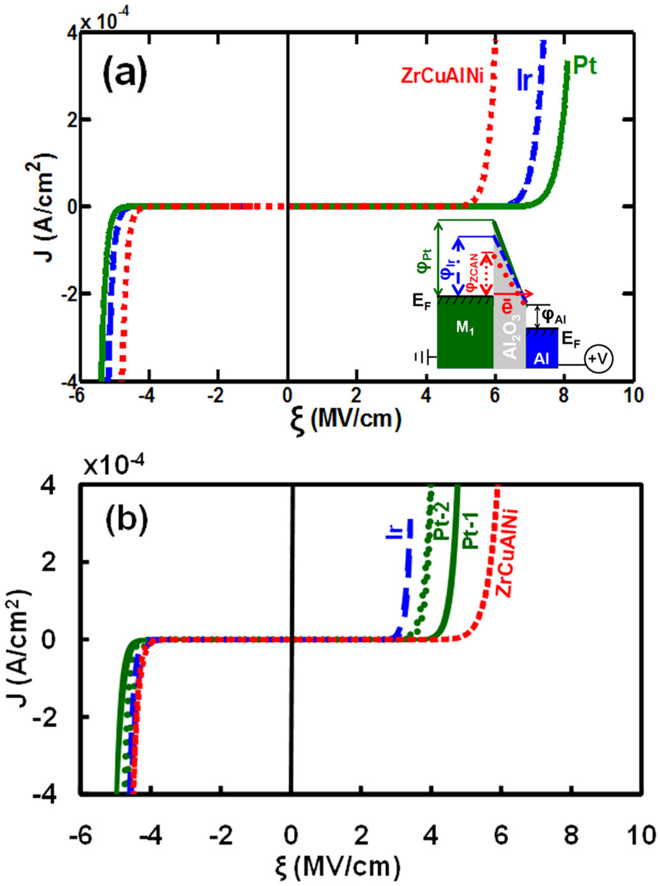

FIG. 2. (Color online) Plots of current density vs electric field (J-ξ) for MIM diodes prepared with 10 nm Al_2O_3 and an Al top (M_2) electrode. (a) Simulated data for diodes with ZrCuAlNi, Ir, and Pt bottom (M_1) electrodes (inset compares band diagrams of diodes with different bottom electrodes under positive bias; ZrCuAlNi is abbreviated as ZCAN). (b) Measured data for devices fabricated using ZrCuAlNi, Ir, sputtered Pt-1, and electron-beam-deposited Pt-2 bottom electrodes.

$$J = \frac{1.1q^2}{4\pi h}\frac{1}{\varphi_b}\left(\frac{V+\Delta\varphi_b}{S}\right)^2 \times \exp\left(\frac{-23\pi\sqrt{qm}}{6h}\varphi_b^{3/2}\left(\frac{S}{V+\Delta\varphi_b}\right)\right), \quad (1)$$

where q is the electron charge, h is Plank's constant, V is the applied bias, φ_b is the barrier height of the electrode-insulator interface from which electrons are tunneling, $\Delta\varphi_b$ is the difference in barrier heights between the interfaces of the insulator with the top and bottom electrodes, m is the effective electron mass, and S is the tunnel barrier thickness. Simulations were performed with MATLAB using an Al_2O_3 thickness of 10 nm, an electron affinity value of 2.58 eV for ALD-Al_2O_3,[19] and an electron effective mass of 0.79 of the free electron mass.[18] The only difference in the three simulated curves is the work function of the bottom electrode (M_1), as given in Table I. In order to understand the J-ξ trends of Fig. 2, it is necessary to consider MIM energy band diagrams. The equilibrium band diagram of a symmetric MIM tunnel device is shown in Fig. 3(a). The J-ξ characteristic of a symmetric MIM device is expected to be symmetric because the barrier to electron tunneling is the same in either direction. The diodes investigated in this work have asymmetric electrodes. The equilibrium band diagram of an asymmetric MIM tunnel diode is shown in Fig. 3(b). φ_{b1} and φ_{b2} indicate the barrier heights of the bottom electrode metal M_1 (Ir, Pt, or ZrCuAlNi) and the smaller work function top gate electrode metal M_2 (Al), respectively. Also shown are band diagrams of the asymmetric diode at the onset of FN tunneling for positive [Fig. 3(c)] and negative [Fig. 3(d)] bias applied to M_2 (assuming that M_1 is grounded).

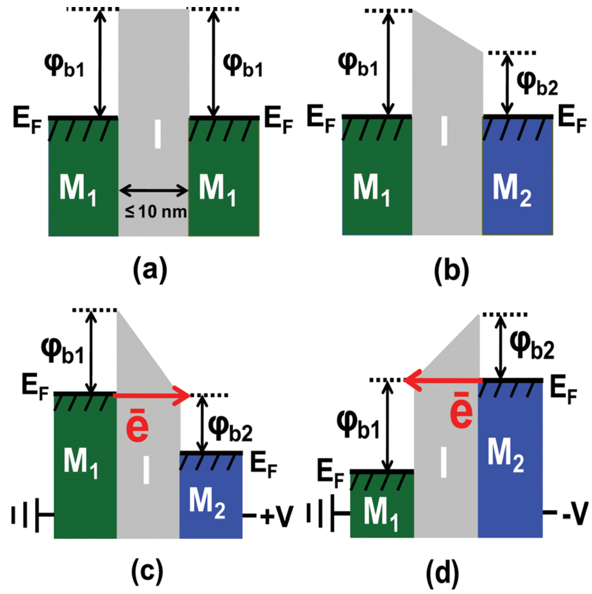

FIG. 3. (Color online) Equilibrium band diagrams of (a) symmetric and (b) asymmetric tunnel diodes. φ_{b1} and φ_{b2} indicate the barrier height of the bottom (high work function) and top (low work function) metal electrodes, respectively. Energy band diagrams of an asymmetric tunnel diode under (c) positive applied bias and (d) negative applied bias at the onset of FN tunneling.

Considering first the application of a sufficiently large *positive* bias to electrode M_2, FN tunnel emission occurs from the bottom electrode (M_1; Ir, Pt, or ZrCuAlNi), with different barrier heights as indicated in the energy band diagram presented in the inset of Fig. 2(a). Note that the sketch is for the applied bias in which tunnel emission from electrode M_1 transitions from direct tunneling (across the entire insulator thickness) to FN tunneling (in which the tunnel distance decreases with increasing bias, because of the now triangular shape of the barrier). Because the insulator thickness used (10 nm) is sufficient to suppress direct tunneling, current conduction is dominated by FN tunneling. The probability of FN tunneling is exponentially dependent upon the insulator thickness and the barrier height presented to the tunneling electron [φ_{b1} for positive biases, as shown in the inset in Fig. 2(a)]. Thus, whereas the *onset* of FN tunneling for positive bias will be roughly the same for all bottom electrodes (as it involves overcoming the same barrier height, φ_{b2}, of the Al top electrode), the magnitude of the FN tunneling current at larger positive fields ($V_{app} \gg \varphi_{b2}$) should be in the reverse order of increasing work function (increasing φ_{b1}). Based on relative barrier heights, the current density of the MIM diode with the ZrCuAlNi electrode

($\Phi_{ZCAN} = 4.8$ eV) would be expected to be higher than that of the device with the Pt electrode ($\Phi_{Pt} = 5.3$ eV), whereas the MIM diode with the Ir electrode ($\Phi_{Ir} = 5.1$ eV) would be intermediate.[20] Although this trend is observed in the simulation [Fig. 2(a)], it is clearly not the trend evidenced in Fig. 2(b), based on the experimental data.

Assuming that the Al_2O_3 thickness for all devices is the same and that conduction is dominated by FN tunneling, a likely explanation for the unexpected trend shown in Fig. 2(b) is associated with the relative roughness of the bottom electrode. A rough bottom electrode could lead to electric field nonuniformity across the insulator due to field enhancement at sharp features, which would decrease the effective insulator thickness. This field enhancement/decreased effective insulator thickness would tend to lead to increased conduction. As shown in Table I for the MIM structures measured in Fig. 2(b), Ir has the largest as-deposited RMS roughness (11 nm), followed by e-beam-deposited Pt-2 (6 nm), sputtered Pt-1 (2 nm), and finally ZrCuAlNi (0.3 nm). As evident from Fig. 2(b), the positive polarity current density trend correlates with the bottom electrode roughness, whereas the curve of the device with a ZrCuAlNi bottom electrode just matches with its simulation.

The RMS roughness for both Ir and Pt-2 are comparable to the overall dielectric thickness. Thus, it is not surprising that the bottom electrode roughness overwhelms the expected influence of the work function. Perhaps the clearest indication of the impact of roughness can be seen by directly comparing MIM tunnel diodes made using the *same* bottom electrode (Pt) with two different levels of roughness. Despite having the same nominal work function, the rougher e-beam evaporated Pt-2 (RMS = 6 nm) device shows a higher positive bias current density than the smoother, dc sputtered Pt-1 (RMS = 2 nm) device [Fig. 2(b)].

Turning next to the application of a sufficiently large *negative* bias to electrode M_2, we see that electron tunnel emission now occurs from the top metal electrode (M_2; Al), as indicated in the energy band diagram in Fig. 3(d). The onset of FN tunneling should not occur until larger negative voltages for larger φ_{b1}, and the simulation in Fig. 2(a) shows that the negative bias current density is expected to decrease slightly with increasing M_1 work function. As shown in the measured data in Fig. 2(b), the devices made with ZrCuAlNi as a bottom electrode once again match fairly well with the simulation. Compared to the simulation, the voltage required in order to achieve a given current density is reduced only slightly for both the Pt and Ir electrode devices. Ir shows the greatest deviation from the simulation, and the rougher Pt-2 once again deviates more than Pt-1.

The deviation between measured and simulated current density is much less on the negative bias side than on the positive bias side (Fig. 2). Additional FN tunneling simulations show that in an asymmetric MIM device, tunneling from the higher work function side (in our case, positive bias tunnel emission from M_1) is more sensitive to changes in the tunnel barrier (such as in thickness, electron effective mass, or electron affinity) than tunneling from the lower work function side (in our case, negative bias tunnel emission from M_2). The data in Fig. 2 suggest that tunneling from the higher work function side (which occurs under positive bias in our experiments) is also more sensitive to roughness than tunneling from the smaller work function side (which occurs under negative bias in our experiments). In addition, some smoothing of the roughest electrodes is observed after ALD (Table I). Whereas the roughness values did not change significantly for ZrCuAlNi and Pt-1, the smoothest as-deposited electrodes, the RMS roughness improved significantly for Ir (from 11 nm to 5 nm) and slightly for Pt-2 (from 6 nm to 5 nm).

The desired J-ξ characteristics for diodes include high nonlinearity and asymmetry. Assuming that FN tunneling dominates, a larger work function difference between electrodes should lead to more nonlinearity and asymmetry, as the simulation in Fig. 2(a) demonstrates. However, this is not the trend observed when roughness dominates, as with the Ir and two Pt electrodes in Fig. 2(b). The largest asymmetry for the experimental J-ξ curves shown in Fig. 2(b) belongs to the diode made with the smoothest electrode—in this case, ZrCuAlNi. The full extent of work function induced asymmetry is evident only when the bottom electrode roughness is minimized.

The percentage of functioning MIM diodes is also found to correlate with bottom electrode roughness. Diodes were considered nonfunctioning when they displayed either electrical shorts or early breakdown under a low applied electric field. Smoother bottom electrodes are found to yield a greater percentage of functioning devices (Table I). Devices fabricated using ZrCuAlNi, the smoothest bottom electrode investigated, have the highest fraction of functioning devices. At the opposite end of the roughness spectrum, no working diodes are obtained using Al bottom electrodes. The Al films are the roughest metal films investigated, with a post-ALD RMS roughness of 21 nm (greater than the tunnel barrier thickness) and a peak roughness of more than 450 nm. For the two types of Pt, the use of the smoother Pt-1 results in a higher percentage of functioning devices than with the rougher Pt-2. Finally, despite having a lower as-deposited and roughly equivalent post-ALD RMS roughness, Pt-2 bottom electrodes are found to yield a lower percentage of working devices than Ir bottom electrodes. This appears to be due to the larger peak roughness of the Pt-2 electrode devices.

Shown in Fig. 4(a) are J-ξ curves for seven Al top electrode (M_2)/$\sim$10 nm thick Al_2O_3 tunnel barrier/ZrCuAlNi bottom electrode (M_1) diodes from five substrates produced in four different process runs. Using ultrasmooth ZrCuAlNi as a bottom electrode, we have been able to produce uniform and repeatable device characteristics with high yield that are well predicted by Fowler-Nordheim tunneling theory and the Simmons equations. Note that despite the inverse dependence of the yield on the bottom electrode roughness and the nonagreement with Fowler-Nordheim theory for the rough bottom electrode devices, when *functioning* devices are obtained, even the devices with a rough bottom electrode (Ir, Pt-1, and Pt-2) exhibit little variation in J-ξ characteristics. Finally, shown in Fig. 4(b) are 100 sequential J-ξ sweeps (-4.5 V to $+6$ V to -4.5 V) on a single Al top electrode (M_2)/$\sim$10 nm thick Al_2O_3 tunnel barrier/ZrCuAlNi bottom electrode (M_1) device, showing a stable J-ξ response.

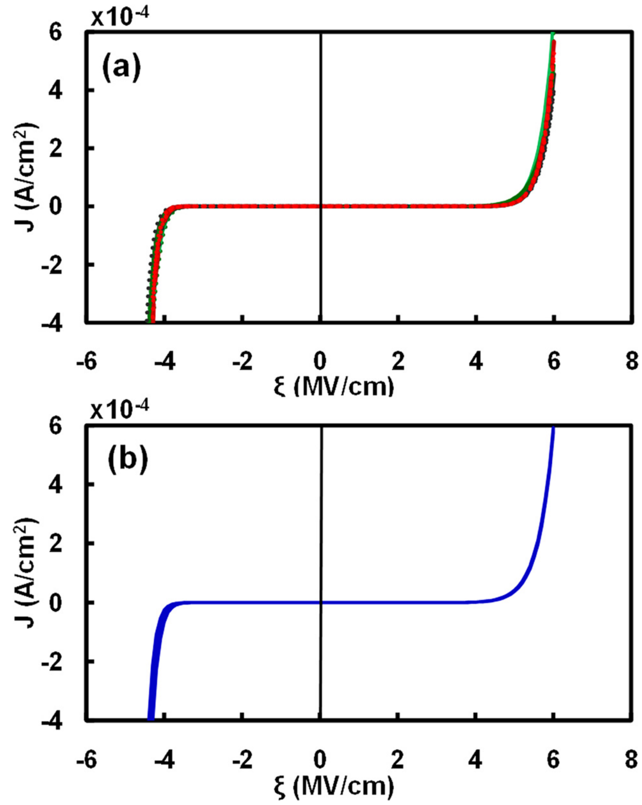

FIG. 4. (Color online) (a) J-ξ sweeps for seven different MIM tunnel diodes taken from five different substrates fabricated in four different identical process runs. Different colors indicate different devices. The fact that the devices overlap and are barely distinguishable from one another is an indication of the run to run and device to device uniformity. (b) One hundred sequential J-ξ sweeps on a single device. In all cases, the stack structure of the devices is ZrCuAlNi/~10 nm Al_2O_3/Al top electrode.

IV. SUMMARY AND CONCLUSIONS

We compare MIM tunnel diode performance on low work function (ZrCuAlNi and Al) and high work function (Ir and two types of Pt) bottom electrode materials with RMS roughness levels ranging from ~3% to greater than 100% of the insulator thickness. Most previous experimental work on MIM diodes has been conducted on native oxides produced by either oxidation or nitridation of the bottom metal electrode. Using ALD, we are able to deposit a high-quality Al_2O_3 insulator independent of the bottom metal electrode. We show (i) that roughness can overwhelm the impact of the metal work function on the electrical characteristics of MIM diodes, in fact reversing the expected trends based on metal work-functions; (ii) that the percentage yield of functioning devices tracks higher with decreasing roughness; and (iii) that even for the same nominal metal (Pt), the level of roughness dominates the electrical properties and yield. Our results indicate that bottom electrode roughness levels of much less than 20% of the insulator thickness are necessary in order to achieve nonroughness dominated electrical behavior, and they suggest that it is likely that most prior MIM tunnel diode studies might have been compromised by uncontrolled bottom electrode roughness.[21] By using ultrasmooth (~0.3 nm RMS) bottom electrodes and uniform tunnel barriers deposited via ALD, we have demonstrated highly nonlinear and asymmetric MIM tunnel diodes with good device to device uniformity and stable J-ξ behavior. The good reproducibility and percentage of working devices, which have been a major challenge for MIM tunnel diodes reported to date, represent an important step toward the commercialization of this technology.

ACKNOWLEDGMENTS

This work was supported in part by grants from the National Science Foundation (through DMR-0805372 and an REU supplement, as well as CHE-0847970), the U.S. Army Research Laboratory (through W911NF-07-2-0083), and the Oregon Nanoscience and Microtechnologies Institute. The authors thank Wei Wang (OSU) for assistance in acquiring AFM images and Cheng Tan for assistance with data collection.

[1] C. A. Mead, J. Appl. Phys. **32**, 646 (1961).
[2] M. Heiblum, Solid-State Electron. **24**, 343 (1981).
[3] J. A. Bean, B. Tiwari, G. H. Bernstein, P. Fay, and W. Porod, J. Vac. Sci. Technol. B **27**, 11 (2009).
[4] S. Krishnan, H. La Rosa, E. Stefanakos, S. Bhansali, and K. Buckle, Sens. Actuators, A **142**, 40 (2008).
[5] W. den Boer, *Active Matrix Liquid Crystal Displays* (Elsevier, Amsterdam, 2005), pp. 43–47.
[6] B. Berland, NREL SR-520-33263 Final Report, 2003.
[7] R. H. Reuss *et al.*, Proc. IEEE **93**, 7 (2005).
[8] S. M. Sze and K. K. Ng, *Physics of Semiconductor Devices*, 3rd ed. (Wiley-Interscience, Hoboken, NJ, 2007), pp. 448–460.
[9] J. G. Simmons, J. Phys. D **4**, 613 (1971).
[10] J. G. Simmons, J. Appl. Phys. **34**, 1793 (1963).
[11] J. G. Simmons, J. Appl. Phys. **34**, 2581 (1963).
[12] C. W. Miller, Z. Li, J. Åkerman, and I. K. Schuller, Appl. Phys. Lett. **90**, 043513 (2007).
[13] P. C. D. Hobbs, R. B. Laibowitz, and F. R. Libsch, Appl. Opt. **44**, 6813 (2005).
[14] Phiar Corp., "A comprehensive source to learn about semiconductor technology," 2010, http://www.phiar.com.
[15] D. Meyerhofer and S. A. Ochs, J. Appl. Phys. **34**, 2535 (1963).
[16] R. M. Handy, Phys. Rev. **126**, 1968 (1962).
[17] P. Periasamy, J. J. Berry, A. A. Dameron, J. D. Bergeson, D. S. Ginley, R. P. O'Hayre, and P. A. Parilla, Adv. Mater. **23**, 3080 (2011).
[18] E. W. Cowell, N. Alimardani, C. C. Knutson, J. F. Conley, Jr., D. A. Keszler, B. J. Gibbons, and J. F. Wager, Adv. Mater. **23**, 74 (2011).
[19] M. L. Hung, Y. C. Chang, C. H. Chang, T. D. Lin, J. Kwo, T. B. Wu, and M. Hong, Appl. Phys. Lett. **89**, 012903 (2006).
[20] H. B. Michaelson, IBM J. Res. Dev. **22**, 72 (1978).
[21] C. B. Duke, *Tunneling in Solids* (Academic Press, New York, 1969), p. 90.